Time-dependent ion transport in heterogeneous permselective systems

Yoav Green and Gilad Yossifon*

Faculty of Mechanical Engineering, Micro- and Nanofluidics Laboratory, Technion–Israel Institute of Technology, Technion City 32000, Israel

(Received 23 March 2015; published 2 June 2015)

The current study extends previous analytical and numerical solutions of chronopotentiometric response of one-dimensional systems consisting of three layers to the more realistic two-dimensional (2D) heterogeneous ion-permselective medium. An analytical solution for the transient concentration-polarization problem, under the local electroneutrality approximation and assumption of ideal permselectivity, was obtained using the Laplace transform and separation of variables technique. Then the 2D electric potential was obtained numerically and was compared to the full Poisson-Nernst-Planck solution. It was then shown that the resultant voltage drop across the system varies between the initial Ohmic response and that of the steady state accounting for concentration polarization. Also, the field-focusing effect in a 2D system is shown to result in a faster depletion of ions at the permselective interface.

DOI: 10.1103/PhysRevE.91.063001 PACS number(s): 47.57.jd, 66.10.Ed, 82.39.Wj

I. INTRODUCTION

The passage of an electric current through a permselective medium (membranes or nanochannels) under an applied electric field is characterized by the formation of concentration gradients, which result in regions of depleted and enriched ionic concentration at opposite ends of the medium [1,2]. The formation of these concentration gradients and the resulting electric current are collectively termed concentration polarization (CP). Initially, in the low-voltage region, the *steady-state* current-voltage (*I-V*) responds in an approximate Ohmic manner. At higher voltages, the current, which is diffusion limited, eventually saturates at a limiting value when the ion concentrations are completely depleted at the permselective interface.

While the steady-state response of the system is of much importance and is used to characterize many attributes of the systems, such as the conductance in the Ohmic region [3–5], in fact it is the dynamical response which can provide much insight on the behavior of the system. From an experimental standpoint, it is crucial to know what the characteristic time scale is during which systems relax so that *I-V* curves can be measured after minimizing time transient effects [6]. Theoretical works have investigated time transient effects in one-dimensional (1D) systems in numerous manners. As far back as 1901, the time-dependent concentration behavior of a solution at the electrode interface was investigated [7–9]. This solution was then rederived for a permselective system of a finite length [10]. Additional analysis for the concentration distribution in a semi-infinite domain, where at infinity the concentration has a bulk value and at the other end there exists a permselective interface, has also been used in numerous works [11]. These solutions have been used to investigate the behavior of the concentration at the interface and the transition time until its complete depletion [12,13]. Also, chronopotentiometry experiments have investigated the time dependency of the electric potential [10,14,15] to a stepwise electric current. A number of works have investigated both the static [16,17] and dynamical [18–20] response of the extended space charge layer (SCL) which forms in the limiting current region.

However, until now, the effects of time-dependent CP phenomena in a realistic heterogeneous three-layered system (i.e., a permselective medium connected by two opposing microchambers—see Fig. 1 for a schematic representation of such a system) has not been theoretically investigated in a thorough manner. In the current study we develop analytical and numerical models to describe time-dependent CP phenomena for heterogeneous permselective systems. Here the term heterogeneity refers to the fact that the size of the permselective interface is smaller than the size of the system (see Fig. 1 and Refs. [21,22] for a complete discussion on heterogeneity in steady state and application related works [23,24]). In particular, the analytical solution is obtained under the assumption of local electroneutrality (LEN), hence, is valid for Ohmic and limiting current conditions, while the numerical solution accounts also for the existence of the SCL. For simplicity we also neglect the surface charge on the microchamber walls and its associated surface-conduction effects [25,26]. In this work we shall focus on solving the electrodiffusive problem in the underlimiting current region which has been proved to be decoupled from the electroconvection problem based on the smallness of the Peclet number for inhomogeneous media [21,22].

In Sec. II we will define the theoretical model and present its solution. In Sec. III we shall provide details regarding the numerical simulations, whereas in Sec. IV we shall go into a lengthy discussion regarding the outcome of our solution. We then give concluding remarks in Sec. V. In an attempt to keep the natural flow of this manuscript unhindered by lengthy mathematical derivations and yet at the same time avoid brevity coming at the expense of completeness, we provide full derivations in the Appendixes.

II. THEORETICAL MODEL

A. Problem definition

The equations governing the time-dependent transport of a symmetric and binary ($z_+ = -z_- = 1$) electrolyte of equal diffusivities ($D_+ = D_- = D$) through a permselective

*Corresponding author: yossifon@tx.technion.ac.il

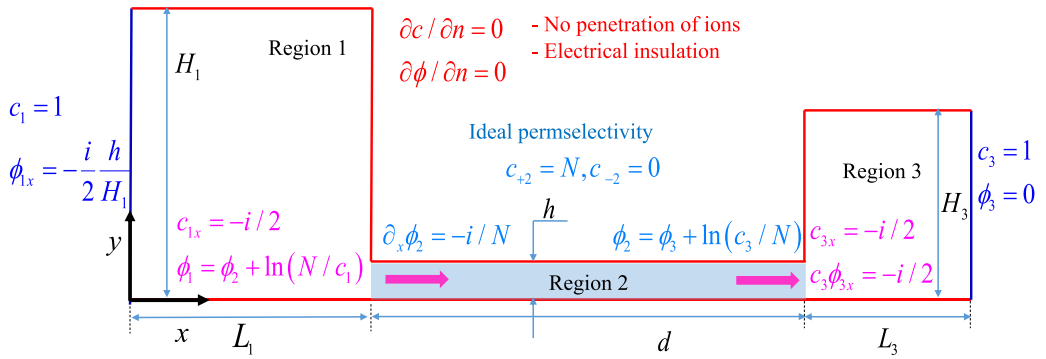

FIG. 1. (Color online) Schematics describing the two-dimensional (2D) geometry of the three-layer system consisting of a straight ideal permselective medium connecting two opposite asymmetric microchambers along with the boundary conditions for the LEN electrodiffusive problem.

medium are the dimensionless Poisson-Nernst-Planck (PNP) equations

$$c_{+,t} = \nabla \cdot [\nabla c_+ + c_+ \nabla \phi] = -\nabla \cdot \boldsymbol{j}_+, \tag{1}$$

$$c_{-,t} = \nabla \cdot [\nabla c_- - c_- \nabla \phi] = -\nabla \cdot \boldsymbol{j}_-, \tag{2}$$

$$\nabla^2 \phi = -\frac{\rho_e}{2\varepsilon^2}, \tag{3}$$

wherein Eqs. (1) and (2) are the Nernst-Planck equations satisfying the continuity of ionic flux conditions. The cationic and anionic concentrations, $\tilde{c}_+$ and $\tilde{c}_-$, respectively, have been normalized by the bulk concentration c_0, where the tilde stands for the parameter in its dimensional form. The spatial coordinates have been normalized by the diffusion length (DL) $\tilde{L}$, the ionic fluxes have been normalized by $\tilde{D}c_0/\tilde{L}$, and the time $\tilde{t}$ has been normalized by the diffusion time $\tilde{L}^2/\tilde{D}$. Equation (3) is the Poisson equation for the electric potential, $\tilde{\phi}$, which has been normalized by the thermal potential RT/F where R is the universal gas constant, T is the absolute temperature, and F is the Faraday constant. The charge density, ρ_e, appearing in Eq. (3) is normalized by zFc_0. The normalized Debye layer is $\varepsilon = \lambda_D/\tilde{L}$, with $\lambda_D = \sqrt{\varepsilon_0 \varepsilon_r RT/2F^2 c_0}$ where ε_0 and ε_r are the permittivity of vacuum and the relative permittivity of the electrolyte, respectively.

Under the LEN approximation [1,2,16,27], one can assume that $\epsilon \ll 1$ (or alternately $\varepsilon^2 \nabla^2 \phi \sim 0$) within the microchambers, thus simplifying the equations. Hence, the Poisson equation [Eq. (3)] can be replaced with the approximation $c_+ = c_- = c$. Addition and subtraction of Eqs. (1) and (2) reduce to

$$c_t = \nabla^2 c, \tag{4}$$

$$\nabla \cdot (c \nabla \phi) = 0. \tag{5}$$

While in the steady-state case the assumption of ideal permselectivity, $\boldsymbol{j}_- = 0$, results in the expression for the electric potential (up to an additive constant)

$$\phi = \ln c, \tag{6}$$

this is clearly not the case for nonsteady transport as $\boldsymbol{j}_- = 0$ holds only at the membrane interface and in a time-dependent problem can vary spatially within the microchambers [see Eq. (2)]. It is noted that the problem of finding the concentration is decoupled from that of the electric potential; hence the concentration is solved first, through Eq. (4), and then the concentration solution is used for solving the electric potential, through Eq. (5).

B. Geometry, boundary, and initial conditions

Our model consists of a three-layer system in which two microchambers are connected by a straight ideal cation-permselective medium, wherein all three domains are of rectangular shape, as shown in Fig. 1. The left microchamber, termed region 1, is defined in the domain $x \in [0, L_1], y \in [0, H_1]$, the permselective medium termed region 2 is defined in the domain $x \in [L_1, L_1 + d], y \in [0, h]$, and the right microchamber termed region 3 is defined in the domain $x \in [L_1 + d, L_1 + d + L_3], y \in [0, H_3]$. Such a geometry realistically describes systems that have been the subject of numerous recent experimental and numerical works [3,4,28–37]. Additionally, this geometry can also describe a periodic array of permselective regions (e.g., nanochannel array or heterogeneous membrane) in the y direction. The spatial coordinates have been normalized by the DL length, $\tilde{L}$ ($\tilde{L}$ can be chosen arbitrarily as either $\tilde{L}_1$ or $\tilde{L}_3$). Without loss of generality, we shall formulate the solution for general values of the dimensionless L_1 and L_3 while we shall remember that at least one of these values when normalized is unity.

Assuming fixed volumetric charge density, N, accounting for the (negative) surface charge within the nanoslot, as in classical models of permselective membranes [36,38], the space charge within all three regions ($n = 1,2,3$) can be written as follows:

$$\rho_{e,n} = c_+ - c_- - N\delta_{n,2}, \tag{7}$$

where $\delta_{n,2}$ is Kronecker's delta. The LEN approximation in the microchambers and cross-sectional electroneutrality within the permselective medium corresponds to $\rho_{e,n} \approx 0$. The case of $N \gg 1$ approximates the conditions of an ideal permselective membrane or nanochannel, requiring that $c_+ \approx N$ and $c_- \approx 0$.

The boundary conditions (BCs) and initial conditions (ICs) are

$$c(x = 0, y, t) = c(x = L_1 + d + L_3, y, t) = 1, \tag{8}$$

$$c_y(x, y = 0, t) = c_y(x, y = H_i, t) = 0, \quad i = 1,3, \tag{9}$$

$$c_x(x = L_1, y, t) = \begin{cases} -i/2 & 0 \leqslant y \leqslant h \\ 0 & \text{else} \end{cases}, \tag{10}$$

$$c_x(x = L_1 + d, y, t) = \begin{cases} -i/2 & 0 \leqslant y \leqslant h \\ 0 & \text{else} \end{cases}, \tag{11}$$

$$c_{1,3}(x, y, t = 0) = 1, \tag{12}$$

where Eq. (8) stands for the stirred bulk electrolyte concentration at the opposite microchannel entrances. Equation (9) is the constraint of no penetration of ions ($\boldsymbol{j}_{\pm} \cdot \boldsymbol{n} = 0$, where n is the coordinate normal to the surface at the solid walls or symmetry planes). Equation (9) is used in conjunction with requiring electrical insulation ($\partial\phi/\partial n = 0$), at the walls or symmetry planes. Equations (10) and (11) are the simplifying assumption of a uniform ionic current density right at the ideal cationic-permselective interface (i.e., $\boldsymbol{j}_- \cdot \boldsymbol{n} = 0$) [21], with i ($= |\boldsymbol{i}|$) being the *uniform* dimensionless current density. In an ideal permselective medium $\tilde{\boldsymbol{i}} = F\tilde{\boldsymbol{j}}_+$, or in dimensionless form $\boldsymbol{i} = \boldsymbol{j}_+$, the current density has been normalized by $F\tilde{D}c_0/\tilde{L}$. Equation (12) is the IC of a uniform bulk concentration within the microchambers under an equilibrium condition. Note that since we are assuming an ideal permselective medium the counterion and coion concentrations within region 2 are fixed in time $c_+ \approx N$ and $c_- \approx 0$, respectively.

C. Concentration solution

Using the Laplace transform, Eq. (4) transforms into the Helmholtz equation. This equation is then solved using a separation of variables technique as described in Appendix A. The solution for the concentration in each region is given by the following expressions:

$$c_1(x,y,t) = 1 - \frac{I}{2H_1}x - \frac{I}{hH_1}\sum_{n=1}^{\infty}\frac{\sin\left(\lambda_n^{(1)}h\right)\cos\left(\lambda_n^{(1)}y\right)\sinh\left(\lambda_n^{(1)}x\right)}{\left(\lambda_n^{(1)}\right)^2\cosh\left(\lambda_n^{(1)}L_1\right)}$$
$$- \frac{I}{H_1L_1}\sum_{m=1}^{\infty}(-1)^m\frac{\sin\left(\gamma_m^{(1)}x\right)}{\left(\gamma_m^{(1)}\right)^2}e^{-\left(\gamma_m^{(1)}\right)^2t} - \frac{2I}{hH_1L_1}\sum_{n,m=1}^{\infty}(-1)^m\frac{\sin\left(\lambda_n^{(1)}h\right)\cos\left(\lambda_n^{(1)}y\right)\sin\left(\gamma_m^{(1)}x\right)e^{-\left(\kappa_{mn}{}^{(1)}\right)^2t}}{\lambda_n^{(1)}\left(\kappa_{mn}{}^{(1)}\right)^2}, \tag{13}$$

$$c_{+,2}(x,y,t) = N, \quad c_{-,2}(x,y,t) = 0, \tag{14}$$

$$c_3(x,y,t) = 1 + \frac{I}{2H_3}(L_1 + d + L_3 - x) + \frac{I}{hH_3}\sum_{n=1}^{\infty}\frac{\sin\left(\lambda_n{}^{(3)}h\right)\cos\left(\lambda_n{}^{(3)}y\right)\sinh\left[\lambda_n{}^{(3)}(L_1 + d + L_3 - x)\right]}{\left(\lambda_n{}^{(3)}\right)^2\cosh\left(\lambda_n{}^{(3)}L_3\right)}$$
$$+ \frac{I}{H_3L_3}\sum_{m=1}^{\infty}(-1)^m\frac{\sin\left[\gamma_m{}^{(3)}(L_1 + d + L_3 - x)\right]}{\left(\gamma_m{}^{(3)}\right)^2}e^{-\left(\gamma_m{}^{(3)}\right)^2t}$$
$$+ \frac{2I}{hH_3L_3}\sum_{n,m=1}^{\infty}(-1)^m\frac{\sin\left(\lambda_n{}^{(3)}h\right)\cos\left(\lambda_n{}^{(3)}y\right)\sin\left[\gamma_m{}^{(3)}(L_1 + d + L_3 - x)\right]e^{-\left(\kappa_{nm}{}^{(3)}\right)^2t}}{\lambda_n{}^{(3)}\left(\kappa_{mn}{}^{(3)}\right)^2}, \tag{15}$$

with the current (normalized by $F\tilde{D}c_0$) and eigenvalues defined as

$$I = ih, \tag{16}$$

$$\lambda_n{}^{(k)} = \frac{\pi n}{H_k}, \quad \gamma_m{}^{(k)} = \frac{\pi(2m-1)}{2L_k}, \quad \kappa_{mn}{}^{(k)} = \sqrt{\left(\lambda_n{}^{(k)}\right)^2 + \left(\gamma_m{}^{(k)}\right)^2}, \tag{17}$$

and the superscript $k = 1,3$ defines the region. The first three terms in Eqs. (13) and (15) are the steady-state solution previously derived in Refs. [5,21,22,39]. The fourth and fifth terms are the time transient solutions corresponding to the 1D transient solution [10] and the 2D field-focusing transient, respectively. In the permselective area the coion and counterion concentrations are held constant. The concentrations at the interface, at $y = 0$, are

$$c_1(x = L_1, y = 0, t) = 1 - \frac{IL_1}{2H_1} - I\bar{f}_1 - I\bar{g}_1(t), \tag{18}$$

$$c_3(x = L_1 + d, y = 0, t) = 1 + \frac{IL_3}{2H_3} + I\bar{f}_3 + I\bar{g}_3(t), \tag{19}$$

$$\bar{f}_k = \frac{1}{hH_k}\sum_{n=1}^{\infty}\frac{\sin\left(\lambda_n{}^{(k)}h\right)\tanh\left(\lambda_n{}^{(k)}L_k\right)}{\left(\lambda_n{}^{(k)}\right)^2}, \tag{20}$$

$$\bar{g}_k(t) = \frac{1}{H_kL_k}\sum_{m=1}^{\infty}\frac{\sin\left(\gamma_m{}^{(k)}L_k\right)}{(-1)^m\left(\gamma_m{}^{(k)}\right)^2}e^{-\left(\gamma_m{}^{(k)}\right)^2t}$$
$$+ \frac{2}{hH_kL_k}\sum_{n,m=1}^{\infty}\frac{\sin\left(\lambda_n{}^{(k)}h\right)\sin\left(\gamma_m{}^{(k)}L_k\right)e^{-\left(\kappa_{mn}{}^{(k)}\right)^2t}}{(-1)^m\lambda_n{}^{(k)}\left(\kappa_{mn}{}^{(k)}\right)^2}, \tag{21}$$

where $\bar{f}_k = \bar{f}_k(L_k, H_k, h)$ represents the steady-state contribution of the field focusing to the solution and is a function of the geometry in each region. The behavior of the $\bar{f}_k$ functions in the varying limits of heterogeneity, i.e., large and small h/H_k, has been recently investigated [22], whereas $\bar{g}_k(t) = \bar{g}_k(t; L_k, H_k, h)$ represents the time transient contribution with the first term representing the 1D decay and the second term representing the 2D decay.

D. Electric potential solution

As previously mentioned, to find the time-dependent electric potential, one must solve Eq. (5), $\nabla \cdot (c\nabla\phi) = 0$. This equation is not explicitly time dependent but rather implicitly through the concentration. A semianalytical solution for the 1D potential drop case is given in Ref. [10] and is rederived in Appendix C to include asymmetric microchannel lengths. In general, Eq. (5) in the 2D case cannot be solved analytically, except at the two extreme cases of $t = 0$ and $t \to \infty$, but rather requires numerical evaluation. The appropriate BCs are (Fig. 1)

$$\phi_x(x = 0, y, t) = -I/2H_1, \quad \phi(x = L_1 + d + L_3, y, t) = 0, \tag{22}$$

$$\phi_y(x, y = 0, t) = \phi_y(x, y = H_i, t) = 0, \quad i = 1,3, \tag{23}$$

$$\phi_x(x = L_1, y, t) = \begin{cases} -i/2c & 0 \leqslant y \leqslant h \\ 0 & \text{else} \end{cases}, \tag{24}$$

$$\phi_x(x = L_1 + d, y, t) = \begin{cases} -i/2c & 0 \leqslant y \leqslant h \\ 0 & \text{else} \end{cases}, \tag{25}$$

$$\phi_{1,3}(x, y, t = 0) = 0, \tag{26}$$

$$\phi_2(x, y, t = 0) = -\ln N, \tag{27}$$

where Eq. (22) is the condition of a grounded side and driving electrical current. Equation (23) is the electrical insulation BC. Equations (24) and (25) are, once more, the simplifying assumption of a uniform ionic current density at the permselective interfaces. Equations (26) and (27) are the IC of a system at equilibrium with the latter being the Donnan potential within the permselective medium. To facilitate the Donnan potential jump we require the continuity of the electrochemical potential of the counterions,

$$\mu_+(x, y, t) = \mu(x, y, t) = \ln c_+(x, y, t) + \phi(x, y, t), \tag{28}$$

at the microchannel-permselective medium interface,

$$\mu_1(x = L_1, y, t) = \mu_2(x = L_1, y, t), \tag{29}$$

$$\mu_2(x = L_1 + d, y, t) = \mu_3(x = L_1 + d, y, t). \tag{30}$$

Solving this problem will yield the desired solution $\phi(x = 0, y, t) = V(t)$. We note here that the coion electrochemical potential of

$$\mu_-(x, y, t) = \ln c_-(x, y, t) - \phi(x, y, t) \tag{31}$$

cannot be used, because in region 2 due to the assumption of ideal permselectivity, $c_- \approx 0$. However, prior to presenting and discussing the numerically computed solution, it is beneficial to discuss the two attainable exact solutions ($t = 0$ and $t \to \infty$). We shall start off with the steady-state solution which was solved in our previous work [5]. For the sake of brevity we shall only give a brief outline of the derivation of the solution. Within an ideal permselective medium the counterions' concentration is constant [Eq. (14)] and under the assumption that the top and bottom surfaces are insulating, we have from the ion-flux continuity equation [Eq. (1)]

$$i = -N\phi_x \Rightarrow \phi_2 = -\frac{I}{Nh}x + \bar{\phi}_2. \tag{32}$$

In general, $\bar{\phi}_2$ is not a constant but is rather time dependent [$\bar{\phi}_2 = \bar{\phi}_2(t)$]. In steady state ($t \to \infty$), where it can be assumed that $\boldsymbol{j}_- = 0$ everywhere and not just within the permselective medium, the potential in the microchambers can be solved from Eq. (2),

$$\phi_1 = \ln c_1 + V, \quad \phi_3 = \ln c_3. \tag{33}$$

The solution for $\bar{\phi}_2$ and an I-V relation can be solved by using the electrochemical continuity requirement given in Eqs. (29) and (30) by requiring continuity at the point $y = 0$ rather than at the entire cross section [5],

$$\bar{\phi}_2 = \frac{I}{hN}(L_1 + d) - \ln N + 2\ln\left(1 + \frac{IL_3}{2H_3} + I\bar{f}_3\right), \tag{34}$$

$$V_s = \frac{Id}{hN} + 2\ln\left[\frac{1 + \frac{IL_3}{2H_3} + I\bar{f}_3}{1 - \frac{IL_1}{2H_1} - I\bar{f}_1}\right], \tag{35}$$

where the subscript s stands for steady-state conditions. In the Ohmic region, for the case of small currents ($I \ll 1$), Eq. (35) is expanded to give the overall steady-state conductance per unit width (normalized by $\tilde{D}F^2c_0/RT$) of the three-layer system,

$$\sigma_s = \frac{1}{R_s} = \frac{I}{V_s} = \left(\frac{d}{hN} + \frac{L_1}{H_1} + \frac{L_3}{H_3} + 2\bar{f}_1 + 2\bar{f}_3\right)^{-1}, \tag{36}$$

and R_s is the system's Ohmic resistance.

At time $t = 0$, prior to application of an electric current, the concentration in each of the regions, excluding the electric double layers (EDLs) interfacing the microchannel-permselective medium interface (LEN approximation), is spatially independent ($c_{1,3} = 1, c_{+,2} = N, c_{-,2} = 0$). Hence the governing equation for the electric potential is reduced from $\nabla \cdot (c\nabla\phi) = 0$ to the Laplace equation,

$$\nabla^2\phi = 0. \tag{37}$$

In Appendix B we derive the solution for the electric potential distribution in all the regions at $t = 0$. The solution differs from the one given in Eqs. (32) and (33). We also derive the initial/rest conductance of the electrolyte as a function of the geometry

$$\sigma_0 = \frac{1}{R_0} = \frac{I}{V_0} = \left(\frac{d}{hN} + \frac{L_1}{2H_1} + \frac{L_3}{2H_3} + \bar{f}_1 + \bar{f}_3\right)^{-1}, \tag{38}$$

where the subscript 0 stands for initial time ($t = 0$) conditions. We note that both Eqs. (36) and (38) are a property of the geometry and permselective counterion concentration. For the sake of generality, following the derivation for $t = 0$ given in Appendix B of this work and in combination for the three-dimensional (3D) potential distribution given in the Appendix of our previous work [5], we provide the initial conductance response given by Eq. (38) for a 3D geometry with

$$\sigma_0 = \frac{1}{R_0} = \frac{I}{V_0} = \left(\frac{d}{Nwh} + \frac{L_1}{2W_1H_1} + \frac{L_3}{2W_3H_3} + \bar{f}_1 + \bar{f}_3\right)^{-1}, \quad (39)$$

with w being the width of the permselective interface and $W_{1,3}$ the width of the according regions (see Fig. 1 of Ref. [5] for a schematic).The full 3D expression for the $\bar{f}$ functions are given by Eq. (26) of Ref. [5].

III. NUMERICAL SIMULATIONS

To verify our results we solved both the LEN approximation (marked by $\varepsilon = 0$ numerical) for the electric potential and the fully coupled PNP equations (marked by $\varepsilon = 10^{-4}$ numerical) given by Eqs. (1)–(3) using the finite elements program COMSOL for the 2D geometry described in Fig. 1. The LEN model was solved using the Partial Differential Equation module, while the PNP equations were solved using the Transport of Diluted Species and Electrostatic modules in COMSOL.

It can be observed from Fig. 1 that, based on the BCs, for the LEN model region 3 can be solved independently of the remaining regions, after which, region 2 can be solved by requiring continuity (with region 3) of the electrochemical potential at the entire interface as given by Eq. (30). Thereafter, using Eq. (29) region 1 is solved. Finally the potential at $\phi(x = 0,y,t) = V(t)$ is evaluated. The LEN numerical model was solved using the BCs specified in Secs. II B and II D. In contrast, the PNP does not require internal BCs at the interfaces between two neighboring regions [such as Eqs. (29) and (30)] as the continuity of ionic fluxes and electric fluxes is accounted for by COMSOL.

Unlike the LEN model ($\varepsilon = 0$), the PNP model ($\varepsilon \neq 0$) accounts for both nonelectroneutral effects (i.e., EDLs and emergence of SCL) and nonideal membrane permselectivity. The IC ($t = 0$) for the PNP simulations, which include the contribution of the EDL, was calculated by applying a zero current, $I = 0$. This equilibrated solution was also used as an initial guess in the current-voltage sweep simulation. Both results will be shown in the following section. We wish to point out that the LEN simulations run substantially quicker (two to three orders of magnitude) than the PNP simulations. This is due to the need to mesh the EDL at the interface in an extremely fine manner which is absent in the LEN simulation. At the two permselective interfaces we use a minimal triangular mesh element of $\varepsilon/30$ with $\varepsilon = 10^{-4}$.

IV. RESULTS AND DISCUSSION

A. Time evolution of concentration polarization

In Fig. 2 the values of time evolution of the concentration profiles for the depleted region are shown for a 1D and 2D (on the center line $y = 0$) case at the limiting current (corresponding to vanishing concentration at the permselective interface in region 1). It is observed that the 2D system reaches its steady-state interfacial value faster than the 1D system. This can be explained due to the following scaling argument of the diffusion equation [Eq. (4)]. The left-hand side scales as $c_0/\tilde{t}$ while the right-hand side scales as $n_d c_0/\tilde{L}^2$ with n_d being the dimensionality of the system. This gives a characteristic time $\tilde{t} \approx \tilde{L}^2/(n_d\tilde{D})$ (in dimensional form) that decreases with increasing n_d. This is also verified in Fig. 3 depicting the time required for the concentration at the interface ($x = L_1$) to reach a quasisteady-state value of $1.001c_s$ [or accordingly from Eq. (18), when $|I\bar{g}_1(t)| = 0.001c_s$]. It is shown that as a system diverges from a homogeneous 1D system ($h = H_{1,3}$)

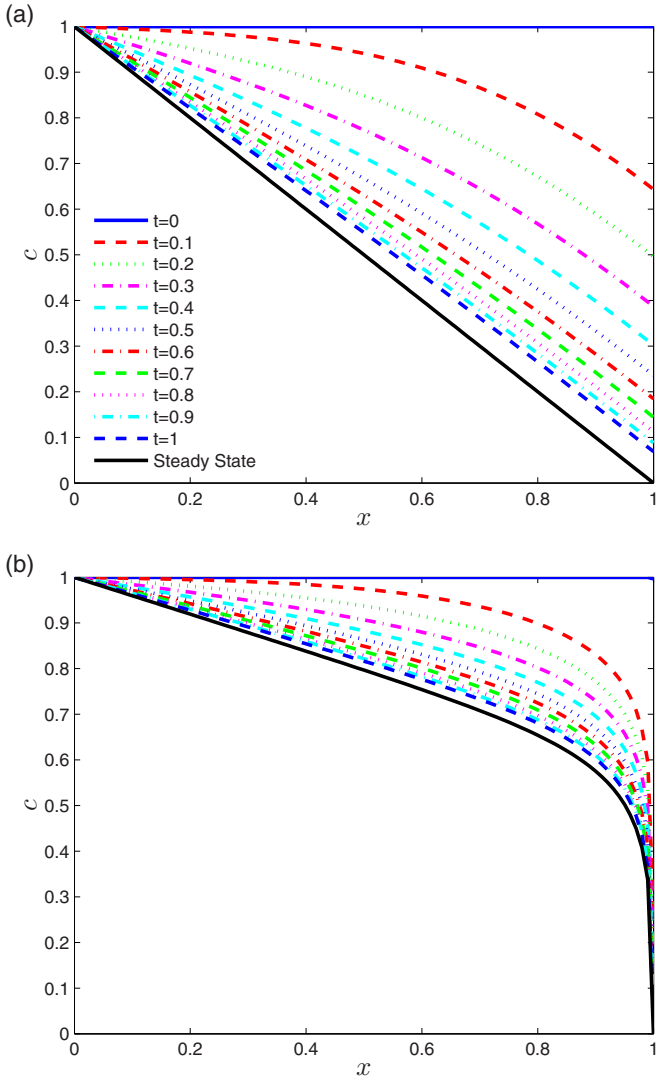

FIG. 2. (Color online) Time-dependent concentration profiles in the depleted region (region 1) at the limiting current density for a (a) 1D system ($i_{\rm lim} = 2$, $h = H$, $L_1 = 1$) and (b) a 2D system ($I_{\rm lim} = 0.322$, $H_1 = 0.4$, $h = 10^{-3}$, $L_1 = 1$).

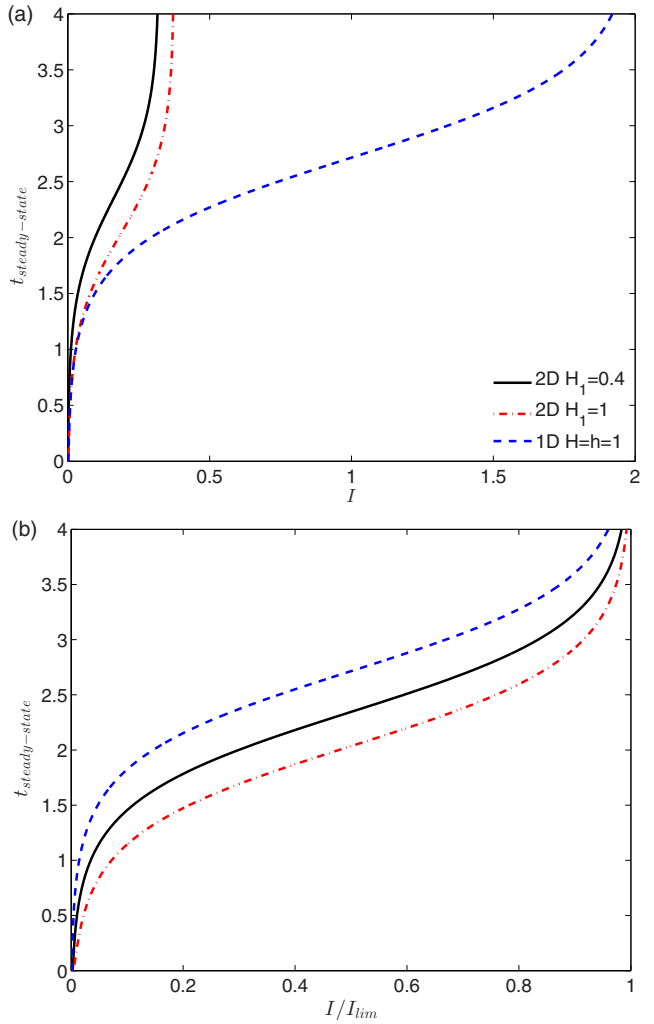

FIG. 3. (Color online) The time to reach a quasisteady state ($1.001c_s$) as a function of the (a) applied current, (b) applied current normalized by the limiting value of each configuration. The plots include the solution for the 1D and 2D cases of ($L_1 = 1$, $H_1 = 1$) and ($L_1 = 1$, $H_1 = 0.4$) with $h = 10^{-3}$, respectively.

into a heterogeneous 2D system the typical time to depletion of ions at the interface decreases. Additionally, we show that this time increases as the current is increased. This is an expected result as for larger currents the degree of depletion increases and more time is required for ions to be removed from the interface. From a mathematical standpoint, it is obvious that the all the $n,m \neq 1$ modes decay quickly; hence it is primarily the $n,m = 1$ that determines the response of the system. In fact, one can observe that the 1D and 2D expressions for the $n,m = 1$ mode in $g(t)$ [Eq. (21)] are of the same sign and thus their contribution is additive. Also, from an intuitive standpoint, the 2D case reaches steady state quicker as the transition is from a uniform concentration of unity to a sharp logarithmic profile, versus the 1D case where the linear profile is achieved. This is explained in the following manner—for $n,m = 1$, the 2D mode dies off quicker than the 1D mode; hence the sole remaining decaying 1D mode reaches the logarithmic profile prior to reaching the linear profile.

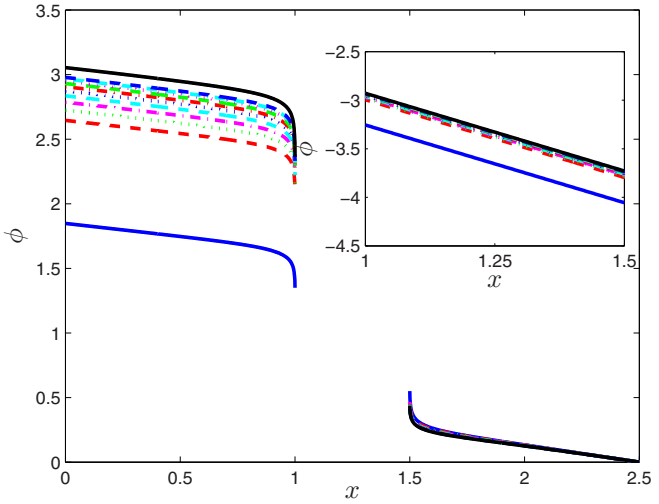

FIG. 4. (Color online) Electric potential profile along the center line ($y = 0$) for the geometry ($L_1 = L_3 = 2d = 1$, $H_1 = 0.4$, $H_3 = 0.3$, $h = 10^{-3}$, $N = 10^2$) at $I_{\text{lim}}/2$. The inset shows the potential within the permselective medium. The legend is that shown in Fig. 2.

B. Time evolution of the electric potential

In Fig. 4 the electric potential as a function of time is plotted in all three regions for a 2D model. The numerically calculated potentials overlap with the analytical solutions for $t = 0$ and $t \to \infty$. Interestingly, it is observed that the potential drop across the anodic and cathodic microchambers is initially similar for the specified geometry. Also observed, the cathodic and the permselective media potential drops do not change substantially over time whereas in contrast, the potential drop within the anodic microchannel (and its associated Donnan jump) increases over time. As a result the total voltage drop across the system $V(t)$ also changes substantially. This corresponds to an increase in the resistance from $t = 0$ [Eq. (38)] to that at steady state, $t \to \infty$ [Eq. (36)]. In actuality, it should be stated that the initial resistance given by Eq. (38) is independent of the current regime (Ohmic or limiting or overlimiting). While Eq. (36) provides a simple expression for the steady-state resistance in the Ohmic region, for larger currents the voltage is nonlinearly dependent on the current and must be evaluated from Eq. (35). Another interesting feature regarding Eqs. (36) and (38) is that the ratio between the steady-state and initial conductance approaches 2 when the permselective medium's resistance, d/hN, vanishes due to the inverse dependence on the fixed volumetric charge N, where in the ideal permselective case $N \gg 1$.

Figure 5 depicts the time evolution of the voltage drop $V(t)$ for both the 1D and 2D cases. The 1D case exhibits an excellent agreement between the LEN simulation ($\varepsilon = 0$) and theoretical prediction for the initial and steady-state cases. For the 1D model, there exists a simpler way to numerically evaluate the potential drop over the entire system $V(t)$. In Appendix C we provide a derivation for a semianalytical expression that needs to be evaluated numerically. The advantage of such a method is that one does not need to resort to numerical simulations. However, 1D simulations are an important stepping stone to

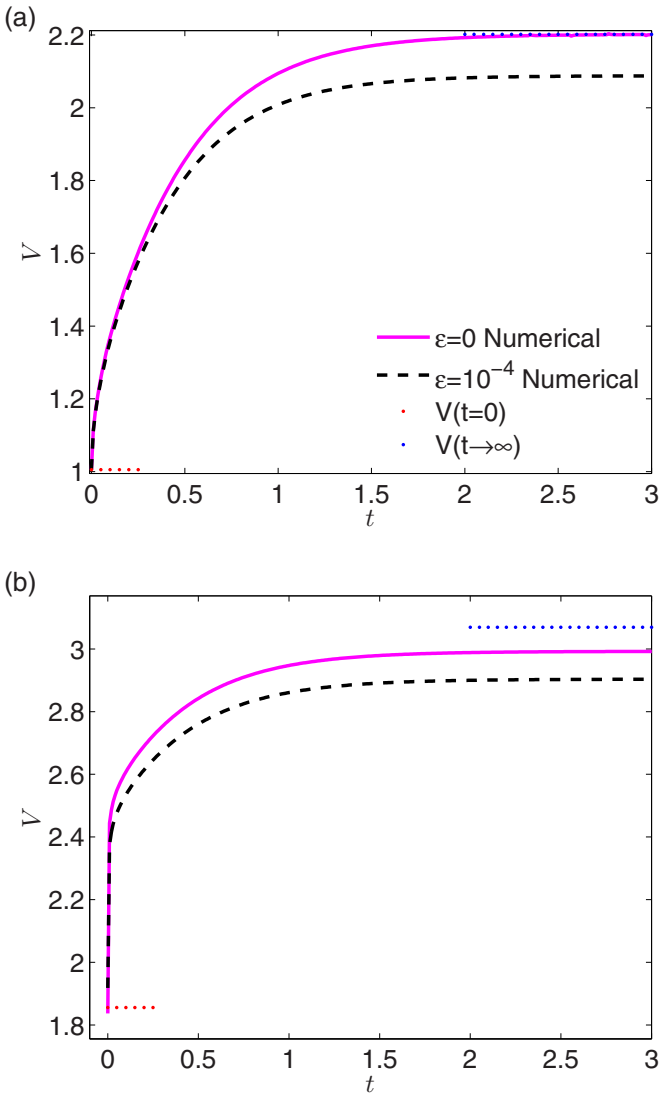

FIG. 5. (Color online) V-t response for the (a) 1D and (b) 2D cases at their respective $0.5I_{\text{lim}}$. The 1D geometry is ($L_1 = L_3 = 1$, $d = 0.5$, $N = 100$) while the 2D geometric details are the same as in Fig. 4.

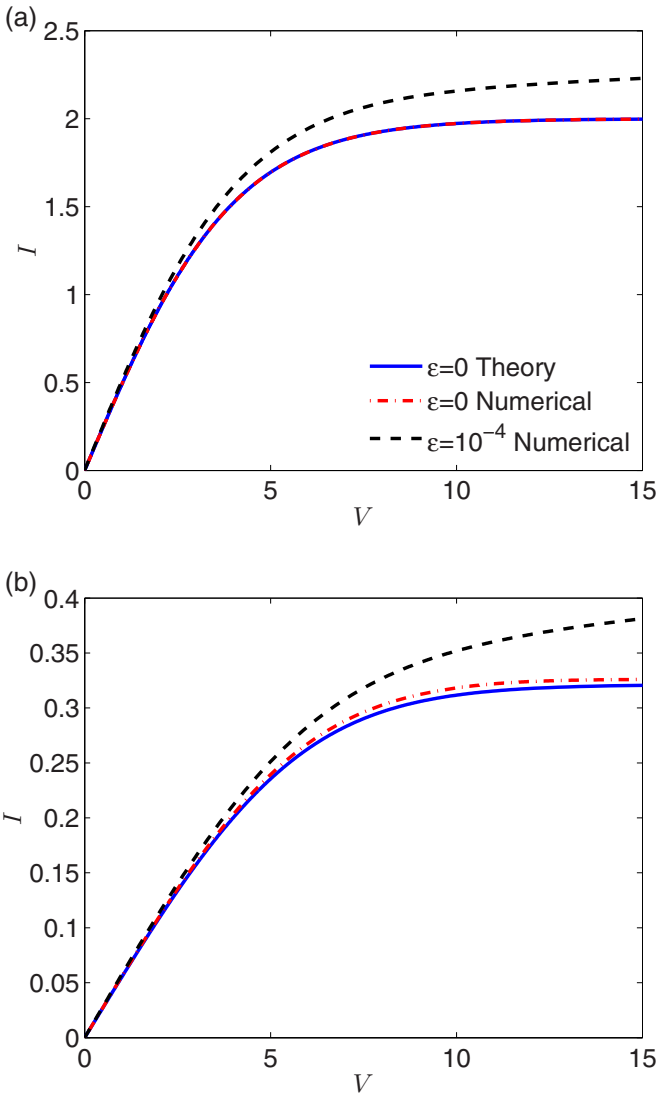

FIG. 6. (Color online) Steady-state I-V curves computed for the LEN approximation and PNP equations for (a) 1D and (b) 2D cases. The geometries are the same as in Figs. 4 and 5.

developing 2D LEN simulations. We have not added this curve in Fig. 3(a) as it completely overlaps the simulated curve given by the solid magenta line.

We shall now explain the observed deviations of the 2D voltage drop [Fig. 5(b)] as well as the deviation due to the loss of LEN (PNP model). In the 2D case the numerical solution underpredicts the theoretical prediction for the steady-state voltage [Fig. 5(b)]. This difference stems from the latter satisfying the electrochemical continuity at a single point at each of the permselective interfaces, while in the simulations, the former satisfies the continuity across the entire permselective medium interface. For the case of solving the fully coupled PNP ($\varepsilon = 10^{-4}$) equations it can be observed that the total voltage drop has a larger deviation from the analytically predicted steady-state result. A similar deviation is also visible in the I-V curves depicted in Fig. 6 (at steady-state conditions). For the 1D case [Fig. 6(a)] the analytical solution, Eq. (35), and the numerical LEN solution are identical and show the expected saturation of the current to the limiting value corresponding to an infinite resistance [1]. At high voltages the PNP solution exhibits a large but finite resistance corresponding to the creation of the SCL [16,17]. This space charge increases the overall conductance of the system relative to that of the LEN conductance. In a complimentary manner this results in a decrease of the resistance of the $\varepsilon = 10^{-4}$ relative to the $\varepsilon = 0$ case. This is also true for the 2D case presented in Fig. 6(b). This also explains the additional decrease of the steady-state resistance depicted in Fig. 5 for the cases of $\varepsilon = 10^{-4}$.

V. CONCLUSIONS

We derived an analytical solution, using the Laplace transform and separation of variable technique, for the temporal-spatial concentration distribution in a 2D three-layered system

[Eqs. (13)–(15)]. We then proceed to investigate the time-dependent behavior exhibited by the system. In steady state the concentration profiles for a 1D and 2D system are linear and logarithmic-like, respectively. Due to the field-focusing effect in a 2D system a faster depletion of ions occurs at the permselective interface corresponding to a decreased characteristic time with increasing dimensionality. We then derived an expression for the initial resistance of the system as a function of the geometry and permselective fixed volumetric charge concentration. In the case where the permselective medium resistance d/hN is substantially lower than the remaining resistors, the ratio between the Ohmic steady-state and initial resistors is $R_s/R_0 = 2$. This is explained due to the fact that in steady state the current is transported only by the positively charged counterions, due to ideal permselectivity of the membrane, where at initial times both the counterions and coions contribute equally to the current. In the limit of vanishing permselectivity, the concentration is constant and uniform throughout the system resulting in an Ohmic response at all times (see Ref. [5] for more details).

The electric potential was then calculated numerically under the LEN approximation as well as solving the fully coupled PNP equations. The two different sets of numerical simulations confirm that the resultant electric potential evolves between the two analytical solutions for $t = 0$ and $t \to \infty$. In particular, we obtained an almost abrupt jump in the potential for the 2D case which is associated with the fast interfacial depletion at the anodic side of the permselective medium. As time evolves the Donnan potential drops across the anodic (cathodic) side of the membrane are increasing (decreasing) as expected from Eqs. (29) and (30), [i.e., $\Delta\phi_{\text{Donnan}} = \ln(N/c_+)$], since the interfacial concentration within the microchamber c_+ is depleted (enriched) with time. In contrast the voltage drop across the permselective medium is constant due to its Ohmic behavior, i.e., constant resistance. It should be pointed out that in two dimensions the numerically calculated resultant voltage is lower than the predicted steady-state response. This is due to the fact that the steady-state theoretical model assumes continuity of the electric potential only at a single point of the permselective interface whereas the numerical model ensures continuity at the entire interface. The difference is best observed in the *I-V* curves which show that a minute difference exists solely in the limiting region.

As suggested in the current study, the measured initial voltage drop of a chronopotentiometric experiment provides, through Eq. (38), a means to extract the effective fixed volumetric charge of the permselective medium, $\tilde{N}$. This is advantageous over the steady-state Ohmic current-voltage response [Eq. (36)] which necessitates slow sweep rates (in relation to the diffusion time scale) of the voltage in order to obtain a quasisteady-state response.

ACKNOWLEDGMENTS

We thank Dr. Sinwook Park and Dr. Ory Schnitzer for fruitful discussions and helpful comments. This work was supported by ISF Grant No. 1078/10. We thank the Technion RBNI (Russell Berrie Nanotechnology Institute) and the Technion GWRI (Grand Water Research Institute) for their financial support.

APPENDIX A: CONCENTRATION SOLUTION DERIVATION

Using the Laplace transform for the time coordinate,

$$C(x,y,s) = \int_0^\infty c(x,y,t)e^{-st}dt, \tag{A1}$$

on Eq. (4) gives

$$sC - c_{t=0} = C_{xx} + C_{yy}, \tag{A2}$$

which is the inhomogeneous Helmholtz equation and $c_{t=0}$ is the initial condition in Eq. (12). The modified BCs for region 1 are

$$C(x = 0,y,s) = 1/s, \tag{A3}$$

$$C_y(x,y = 0,s) = C_y(x,y = H_1,s) = 0, \tag{A4}$$

$$C_x(x = L_1,y,s) = \begin{cases} -i/(2s), & 0 \leqslant y \leqslant h \\ 0, & \text{else} \end{cases}. \tag{A5}$$

A separation of variables method,

$$C_h(x,y,s) = X(x,s)Y(y,s), \tag{A6}$$

is used to solve the homogeneous equation in Eq. (41). It is clear from Eq. (A6) that all functions are explicitly dependent on s, yet for the sake of brevity, from this point on we shall write this implicitly. Inserting Eq. (A6) in Eq. (A2) gives

$$s - \frac{X''(x)}{X(x)} = \frac{Y''(y)}{Y(y)} = -\lambda^2. \tag{A7}$$

The solution of Eq. (A7) is

$$Y = A\cos(\lambda y) + B\sin(\lambda y). \tag{A8}$$

Use of BC Eq. (A4) gives

$$B = 0,\ \ \lambda_n = \pi n/H_1,\ \ n = 1,2,3\cdots, \tag{A9}$$

so that

$$Y_n(y) = A_n\cos(\lambda_n y). \tag{A10}$$

For the case $\lambda^2 = n = 0$, it is easy to see that the $Y_{n=0} = A_0$ and the governing equation and its solution are

$$sC_0 - c_{t=0} = C_{0xx}, \tag{A11}$$

$$C_0 = E_0\sinh(\sqrt{s}x) + F_0\cosh(\sqrt{s}x) + \frac{1}{s}, \tag{A12}$$

where we have added the inhomogeneous component $c_{t=0}$ which gives the $1/s$ term. Then from Eqs. (A7) and (A9) one obtains

$$X_n(x) = E_n\sinh\left(\sqrt{{\lambda_n}^2 + s}x\right) + F_n\cosh\left(\sqrt{{\lambda_n}^2 + s}x\right). \tag{A13}$$

Hence the complete solution is

$$\begin{aligned} C(x,y,s) = {} & \frac{1}{s} + E_0\sinh(\sqrt{s}x) + F_0\cosh(\sqrt{s}x) \\ & + \sum_{n=1}^{\infty}\left[E_n\sinh\left(\sqrt{{\lambda_n}^2 + s}x\right)\right. \\ & \left. + F_n\cosh\left(\sqrt{{\lambda_n}^2 + s}x\right)\right]\cos\lambda_n y. \end{aligned} \tag{A14}$$

Use of BC Eq. (A3) requires that

$$F_0 = 0, \quad F_n = 0. \tag{A15}$$

For the BC of current flux density conservation [Eq. (A5)], we then take the x derivative of Eq. (A14) and find the Fourier coefficients,

$$\begin{aligned} E_0 &= -\frac{I}{2H_1 s\sqrt{s}\cosh(\sqrt{s}L_1)}, \\ E_n &= -\frac{I\sin(\lambda_n h)}{\lambda_n H_1 h s\sqrt{{\lambda_n}^2+s}\cosh\left(\sqrt{{\lambda_n}^2+s}L_1\right)}, \end{aligned} \tag{A16}$$

with $I = ih$. Inserting Eqs. (A15) and (A16) into Eq. (A14) gives

$$\begin{aligned} C(x,y,s) &= \frac{1}{s} - \frac{I\sinh(\sqrt{s}x)}{2H_1 s\sqrt{s}\cosh(\sqrt{s}L_1)} \\ &\quad - \frac{I}{H_1 h}\sum_{n=1}^{\infty}\left[\frac{\sin(\lambda_n h)\sinh\left(\sqrt{{\lambda_n}^2+s}x\right)\cos(\lambda_n y)}{\lambda_n s\sqrt{{\lambda_n}^2+s}\cosh\left(\sqrt{{\lambda_n}^2+s}L_1\right)}\right]. \end{aligned} \tag{A17}$$

We calculate the inverse Laplace transform using the residue theorem,

$$\begin{aligned} c(x,y,t) &= \frac{1}{2\pi j}\lim_{T\to\infty}\int_{\alpha-jT}^{\alpha+jT} C(x,y,s)e^{st}ds \\ &= \mathrm{Res}[C(x,y,s)e^{st},s_l], \end{aligned} \tag{A18}$$

for all $t > 0$, where s_l is a pole of $C(x,y,s)$ and j is the imaginary unit. The first term in Eq. (A17) has a single pole at $s = 0$ yielding

$$c_{\mathrm{I}}(x,y,t) = 1. \tag{A19}$$

The second term has one pole at $s = 0$ and an infinite series of poles,

$$s_m = -\frac{\pi^2(2m-1)^2}{4L_1^2} = -\gamma_m^2, \quad m = 1,2,3\cdots. \tag{A20}$$

Thus, yielding from the second term in Eq. (A17),

$$c_{\mathrm{II}}(x,y,t) = -\frac{I}{2H_1}x - \frac{I}{H_1 L_1}\sum_{m=1}^{\infty}\frac{\sin(\gamma_m x)}{{\gamma_m}^2\cos(\pi m)}\mathrm{e}^{-{\gamma_m}^2 t}. \tag{A21}$$

The term $\cos\pi m$ is simply $(-1)^m$. Finally the third term has poles at $s = 0$ and

$$s_{mn} = -\gamma_m^2 - \lambda_n^2 = -\kappa_{mn}^2, \quad m = 1,2,3\cdots, \quad n = 1,2,3\cdots, \tag{A22}$$

transforming the third term of Eq. (A17) into

$$c_{\mathrm{III}}(x,y,t) = -\frac{I}{H_1 h}\sum_{n=1}^{\infty}\frac{\sin(\lambda_n h)\cos(\lambda_n y)\sinh(\lambda_n x)}{{\lambda_n}^2\cosh(\lambda_n L_1)} - \frac{2I}{L_1 H_1 h}\sum_{n,m=1}^{\infty}\frac{\sin(\lambda_n h)\cos(\lambda_n y)\sin(\gamma_m x)\mathrm{e}^{-{\kappa_{mn}}^2 t}}{\lambda_n\left({\gamma_m}^2+{\lambda_n}^2\right)\cos(\pi m)}. \tag{A23}$$

Then the solution for the concentration in region 1 is the sum of Eqs. (A19), (A21), and (A23),

$$\begin{aligned} c_1(x,y,t) &= 1 - \frac{I}{2H_1}x - \frac{I}{hH_1}\sum_{n=1}^{\infty}\frac{\sin\left(\lambda_n^{(1)}h\right)\cos\left(\lambda_n^{(1)}y\right)\sinh\left(\lambda_n^{(1)}x\right)}{\left(\lambda_n^{(1)}\right)^2\cosh\left(\lambda_n^{(1)}L_1\right)} \\ &\quad - \frac{I}{H_1 L_1}\sum_{m=1}^{\infty}(-1)^m\frac{\sin\left(\gamma_m^{(1)}x\right)}{\left(\gamma_m^{(1)}\right)^2}\mathrm{e}^{-\left(\gamma_m^{(1)}\right)^2 t} - \frac{2I}{hH_1 L_1}\sum_{n,m=1}^{\infty}(-1)^m\frac{\sin\left(\lambda_n^{(1)}h\right)\cos\left(\lambda_n^{(1)}y\right)\sin\left(\gamma_m^{(1)}x\right)\mathrm{e}^{-\left(\kappa_{nm}^{(1)}\right)^2 t}}{\lambda_n^{(1)}\left(\kappa_{nm}^{(1)}\right)^2}. \end{aligned} \tag{A24}$$

We note that for the case $h = H_1$, the 2D transient solution reverts to the 1D solution given in Ref. [10]. Similarly to the above shown procedure one can find the solution for region 3 using the relevant BCs.

APPENDIX B: INITIAL ELECTRIC POTENTIAL SOLUTION

At $t = 0$ when the concentration in each of the regions is uniform the equation governing the electric potential within the microchambers, outside EDLs at the microchannel-permselective medium interface, is simply the Laplace equation,

$$\nabla^2\phi = 0. \tag{B1}$$

Given that the BCs, previously given in Sec. II D, for the electric potential are similar to the BCs of the concentration given in Sec. II B, this suggests that the electric potential solution has a similar form to that of the concentration (as was previously shown in Ref. [5] which solved a similar problem governed by the Laplace equation, albeit a different physical situation). It can

be shown that the electric potential in region 3 is

$$\phi_3(x,y) = \frac{I}{2H_3}(L_1+d+L_3-x) + \frac{I}{hH_3}\sum_{n=1}^{\infty}\frac{\sin {\lambda_n}^{(3)}h \sinh\left[{\lambda_n}^{(3)}(L_1+d+L_3-x)\right]\cos {\lambda_n}^{(3)}y}{\left({\lambda_n}^{(3)}\right)^2\cosh\left({\lambda_n}^{(3)}L_3\right)}. \tag{B2}$$

The electric potential in region 2 remains unchanged,

$$\phi_2(x,y) = -\frac{I}{Nh}x + \bar{\phi}_{2,0}, \tag{B3}$$

and requiring continuity of electrochemical potential [Eq. (30)] gives

$$\bar{\phi}_{2,0} = \frac{I}{hN}(L_1+d) - \ln N + \frac{IL_3}{2H_3} + I\bar{f}_3. \tag{B4}$$

The potential in region 1 is accordingly

$$\phi_1(x,y,t) = V_0 - \frac{I}{2H_1}x - \frac{I}{H_1 h}\sum_{n=1}^{\infty}\frac{\sin\left({\lambda_n}^{(1)}h\right)\sinh\left({\lambda_n}^{(1)}x\right)\cos\left({\lambda_n}^{(1)}y\right)}{\left({\lambda_n}^{(1)}\right)^2\cosh\left({\lambda_n}^{(1)}L_1\right)}. \tag{B5}$$

The initial potential jump, V_0, at time $t=0$ can be found using Eq. (29), yielding

$$V_0 = I\left(\frac{d}{Nh} + \frac{L_1}{2H_1} + \frac{L_3}{2H_3} + \bar{f}_1 + \bar{f}_3\right), \tag{B6}$$

which corresponds to an initial conductance of

$$\sigma_0 = \frac{I}{V_0} = \left(\frac{d}{Nh} + \frac{L_1}{2H_1} + \frac{L_3}{2H_3} + \bar{f}_1 + \bar{f}_3\right)^{-1}. \tag{B7}$$

APPENDIX C: 1D TIME-DEPENDENT VOLTAGE DERIVATION

In this Appendix we shall derive an expression for the potential drop over the entire system for the 1D case. A solution for the potential drop over the entire system for the 1D case was previously presented in Ref. [10]. For completeness reasons we rederive the expression and extend it to the case of nonsymmetric microchamber lengths. We also include an expression for the permselective region medium resistance which was not included in previous works. Following Eq. (5), the potential drop over region 3 is given by the integral

$$\Delta\phi_3(t) = -\int_{L_1+d}^{L_1+d+L_3}\frac{i}{2c_3(x,t)}dx. \tag{C1}$$

The potential drop over the permselective medium remains unchanged during the transition phase,

$$\Delta\phi_2 = -i\frac{d}{N}, \tag{C2}$$

while the Donnan potential drops at the opposite interface are obtained, using Eqs. (29) and (30), as

$$\Delta\phi_{D23} = \ln\left[\frac{N}{c_3(x=L_1+d,t)}\right], \tag{C3}$$

$$\Delta\phi_{D12} = \ln\left[\frac{c_1(x=L_1,t)}{N}\right], \tag{C4}$$

leading to a total Donnan potential drop *difference* of

$$\Delta\phi_D = \ln\left[\frac{c_1(x=L_1,t)}{c_3(x=L_1+d,t)}\right]. \tag{C5}$$

Similarly, the potential drop in region 1 is

$$\Delta\phi_1(t) = -\int_0^{L_1}\frac{i}{2c_1(x,t)}dx. \tag{C6}$$

Thus the voltage drop over the entire system is simply

$$\Delta\phi(t) = \Delta\phi_1 + \Delta\phi_2 + \Delta\phi_3 + \Delta\phi_D, \tag{C7}$$

which can be written specifically

$$V(t) = -\Delta\phi(t) = \int_0^{L_1}\frac{i}{2c_1(x,t)}dx + i\frac{d}{N} + \int_{L_1+d}^{L_1+d+L_3}\frac{i}{2c_3(x,t)}dx - \ln\left[\frac{c_1(x=L_1,t)}{c_3(x=L_1+d,t)}\right]. \tag{C8}$$

[1] V. G. Levich, *Physicochemical Hydrodynamics* (Prentice-Hall, New York, 1962).

[2] I. Rubinstein, *Electro-Diffusion of Ions* (SIAM, Philadelphia, 1990).

[3] D. Stein, M. Kruithof, and C. Dekker, Surface-charge-governed ion transport in nanofluidic channels, Phys. Rev. Lett. **93**, 035901 (2004).

[4] R. B. Schoch, H. van Lintel, and P. Renaud, Effect of the surface charge on ion transport through nanoslits, Phys. Fluids **17**, 100604 (2005).

[5] Y. Green, S. Shloush, and G. Yossifon, Effect of geometry on concentration polarization in realistic heterogeneous permselective systems, Phys. Rev. E **89**, 043015 (2014).

[6] D. Deng, E. V. Dydek, J.-H. Han, S. Schlumpberger, A. Mani, B. Zaltzman, and M. Z. Bazant, Overlimiting current and shock electrodialysis in porous media, Langmuir **29**, 16167 (2013).

[7] H. J. S. Sand, On the concentration at the electrodes in a solution, with special reference to the liberation of hydrogen by electrolysis of a mixture of copper sulphate and sulphuric acid, Proc. Phys. Soc., London **17**, 496 (1899).

[8] H. F. Weber, LXI. Researches on the elementary law of hydrodiffusion, Philos. Mag., Ser. 5 **8**, 523 (1879).

[9] E. V. Dydek and M. Z. Bazant, Nonlinear dynamics of ion concentration polarization in porous media: The leaky membrane model, AIChE J. **59**, 3539 (2013).

[10] P. Sistat and G. Pourcelly, Chronopotentiometric response of an ion-exchange membrane in the underlimiting current-range. Transport phenomena within the diffusion layers, J. Membr. Sci. **123**, 121 (1997).
[11] H.-W. Rösler, F. Maletzki, and E. Staude, Ion transfer across electrodialysis membranes in the overlimiting current range: chronopotentiometric studies, J. Membr. Sci. **72**, 171 (1992).
[12] M. Svoboda, Z. Slouka, W. Schrott, and D. Šnita, Cation exchange membrane integrated into a microfluidic device, Microelectron. Eng. **86**, 1371 (2009).
[13] J. J. Krol, M. Wessling, and H. Strathmann, Chronopotentiometry and overlimiting ion transport through monopolar ion exchange membranes, J. Membr. Sci. **162**, 155 (1999).
[14] C. Larchet, S. Nouri, B. Auclair, L. Dammak, and V. Nikonenko, Application of chronopotentiometry to determine the thickness of diffusion layer adjacent to an ion-exchange membrane under natural convection, Adv. Colloid Interface Sci. **139**, 45 (2008).
[15] J.-H. Choi, S.-H. Kim, and S.-H. Moon, Heterogeneity of ion-exchange membranes: The effects of membrane heterogeneity on transport properties, J. Colloid Interface Sci. **241**, 120 (2001).
[16] I. Rubinstein and L. Shtilman, Voltage against current curves of cation exchange membranes, J. Chem. Soc., Faraday Trans. 2 **75**, 231 (1979).
[17] E. Yariv, Asymptotic current-voltage relations for currents exceeding the diffusion limit, Phys. Rev. E **80**, 051201 (2009).
[18] I. Rubinstein, B. Zaltzman, A. Futerman, V. Gitis, and V. Nikonenko, Reexamination of electrodiffusion time scales, Phys. Rev. E **79**, 021506 (2009).
[19] I. Rubinstein and B. Zaltzman, Probing the extended space charge by harmonic disturbances, Phys. Rev. E **80**, 021505 (2009).
[20] I. Rubinstein and B. Zaltzman, Dynamics of extended space charge in concentration polarization, Phys. Rev. E **81**, 061502 (2010).
[21] I. Rubinstein, Electroconvection at an electrically inhomogeneous permselective interface, Phys. Fluids A **3**, 2301 (1991).
[22] Y. Green and G. Yossifon, Effects of three-dimensional geometric field focusing on concentration polarization in a heterogeneous permselective system, Phys. Rev. E **89**, 013024 (2014).
[23] N. A. Mishchuk, Polarization of systems with complex geometry, Curr. Opin. Colloid Interface Sci. **18**, 137 (2013).
[24] N. A. Mishchuk, Concentration polarization of interface and non-linear electrokinetic phenomena, Adv. Colloid Interface Sci. **160**, 16 (2010).
[25] E. V. Dydek, B. Zaltzman, I. Rubinstein, D. S. Deng, A. Mani, and M. Z. Bazant, Overlimiting Current in a Microchannel, Phys. Rev. Lett. **107**, 118301 (2011).
[26] A. Mani and M. Z. Bazant, Deionization shocks in microstructures, Phys. Rev. E **84**, 061504 (2011).
[27] B. Zaltzman and I. Rubinstein, Electro-osmotic slip and electroconvective instability, J. Fluid Mech. **579**, 173 (2007).
[28] G. Yossifon and H.-C. Chang, Selection of nonequilibrium overlimiting currents: Universal depletion layer formation dynamics and vortex instability, Phys. Rev. Lett. **101**, 254501 (2008).
[29] G. Yossifon, P. Mushenheim, and H.-C. Chang, Controlling nanoslot overlimiting current with the depth of a connecting microchamber, Europhys. Lett. **90**, 64004 (2010).
[30] Y. Green and G. Yossifon, Dynamical trapping of colloids at the stagnation points of electro-osmotic vortices of the second kind, Phys. Rev. E **87**, 033005 (2013).
[31] A. Mani, T. A. Zangle, and J. G. Santiago, On the propagation of concentration polarization from microchannel−nanochannel interfaces Part I: Analytical model and characteristic analysis, Langmuir **25**, 3898 (2009).
[32] T. A. Zangle, A. Mani, and J. G. Santiago, On the propagation of concentration polarization from microchannel−nanochannel interfaces Part II: Numerical and experimental study, Langmuir **25**, 3909 (2009).
[33] L.-J. Cheng and L. J. Guo, Rectified ion transport through concentration gradient in homogeneous silica nanochannels, Nano Lett. **7**, 3165 (2007).
[34] B. Kim, J. Heo, H. J. Kwon, S. J. Cho, J. Han, S. J. Kim, and G. Lim, Tunable ionic transport for a triangular nanochannel in a polymeric nanofluidic system, ACS Nano **7**, 740 (2013).
[35] G. Yossifon, P. Mushenheim, Y.-C. Chang, and H.-C. Chang, Nonlinear current-voltage characteristics of nanochannels, Phys. Rev. E **79**, 046305 (2009).
[36] J. A. Manzanares, W. D. Murphy, S. Mafe, and H. Reiss, Numerical simulation of the nonequilibrium diffuse double layer in ion-exchange membranes, J. Phys. Chem. **97**, 8524 (1993).
[37] G. Yossifon, P. Mushenheim, Y.-C. Chang, and H.-C. Chang, Eliminating the limiting-current phenomenon by geometric field focusing into nanopores and nanoslots, Phys. Rev. E **81**, 046301 (2010).
[38] T. Teorell, An attempt to formulate a quantitative theory of membrane permeability, Exp. Biol. Med. (Maywood) **33**, 282 (1935).
[39] I. Rubinstein, B. Zaltzman, and T. Pundik, Ion-exchange funneling in thin-film coating modification of heterogeneous electrodialysis membranes, Phys. Rev. E **65**, 041507 (2002).